IIETA International Information and Engineering Technology Association
Advancing the World of Information and Engineering

Annales de Chimie - Science des Matériaux
Vol. 48, No. 3, June, 2024, pp. 331-339
Journal homepage: http://iieta.org/journals/acsm

Corrosion Mechanism of A333 and API 5L in 0.02 M Acidic Crude Oil Using Sodium Sulfite - Ginger Extract as Inhibitor at Different Temperature and Fluid Velocity of the Medium

Badiea Abdullah Mohamad[1,2*], Kikkeri Naradimha Mohana[3]

[1] Department of Chemical Engineering, Faculty of Engineering, Soran University, Erbil 44008, Iraq
[2] Department of Industrial and Manufacturing System Engineering, Faculty of Engineering, Taiz University, Taiz 004, Yemen
[3] Department of Studies in Engineering Chemistry, University of Mysore, Mysuru 570006, India

Corresponding Author Email: badiea.mahyoub@cheme.soran.edu.iq

https://doi.org/10.18280/acsm.480304

Received: 1 March 2024
Revised: 17 May 2024
Accepted: 4 June 2024
Available online: 30 June 2024

Keywords:
acid corrosion, potentiostatic, acid inhibition, alloy, weight loss

ABSTRACT

A333 and API 5L steel are typical metals used in oil and gas industries. Techniques of gravimetric method, linear polarization resistance, and EIS measurements have been used to examine the synergistic corrosion inhibition performance of sodium sulfite, SS, and ginger extract, GE, on aforementioned metal dissolution in 0.02 M acidic crude oil in pipelines at various temperatures, fluid velocities which is new parameter in term of corrosion studies and could be considered as novel study, and inhibitor concentrations. Moreover, the combination of SS and GE and using them as a synergistic corrosion inhibitor in the acidic crude oil medium could be considered as a novelty. The results remarkably reveal enchantment of SS-GE inhibitory by mitigating metal attack of anodic area by providing polarization to become cathodic surface. Effect of temperature and fluid velocity on the thermodynamic adsorption equilibrium was evaluated and obeys Freundlich isotherm at all studied temperature. Unsignificant temperature effect can be seen.

1. INTRODUCTION

One of the main ways to prevent metal corrosion is a synergistic corrosion inhibitor. It is crucial to investigate how the formed film or adsorption process and corrosion inhibition interact since adsorption determines how protected a metal behaves. The structure of the suggested inorganic and ginger extract inhibitors are shown in Figure 1.

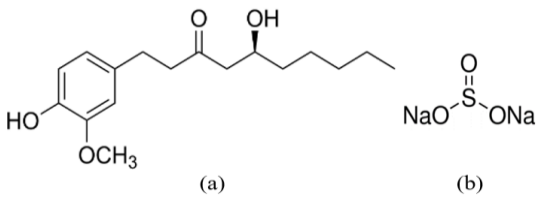

Figure 1. (a) structure of ginger; and (b) sodium sulfite

The primary issue with A333 and API 5L metal used is its tendency strongly to dissolve in the acidic medium. In our study, inorganic sodium sulfite (SS) and ginger extract (GE) synergistic inhibitors were used. A combination of sodium nitrite and borax has been investigated to see how it affects the corrosion of low carbon steel in an industrial water medium at different temperatures, concentrations of the inhibitors, and rotating speeds of the specimens [1]. When ginger and grapefruit oil extracts were used to stop mild steel from corroding in a diluted electrolyte of 0.5 M H_2SO_4, potentiodynamic polarization revealed that the extract dramatically decreased mild steel corrosion from 8.43 mmpy at blank concentration to 0.565 mmpy [2].

Low carbon steel's corrosion mechanism was examined in the presence of volatile inhibitors including organic inhibitors, with respect to temperature and fluid velocity [3]. Several studies have currently investigated the corrosion prevention efficacy and mechanisms of various plant extracts for mild steel [4-6]. The synergic corrosion inhibition role of different compounds of *Mangifera indica* L. Extract and zinc cations was studied by combined electrochemical and computational methods [7]. Inhibitory of steel corrosion by rice straw extract in 3.5% sodium chloride was investigated [8].

Royani et al. [9] investigated the inhibitory potential of Tinospora Cordifolia extract with different methanolic solvents on the corrosion of carbon steel in an artificial seawater environment. In the absence and presence of 2-hydrazino benzothiazole, effect of fluid velocity and temperature on the corrosion mechanism of low carbon steel in industrial water was studied [10]. The corrosion behavior of low-carbon steel in the medium of industrial water and adsorption isotherm of thermodynamics in the presence of plant extracts was investigated [11]. Al-Amiery et al. [12] reviewed the natural and synthetic organic inhibitors. They focused on synthesized and natural organic corrosion inhibitors and their types, active functional groups, and efficiency estimations. Abdallah et al. [13] reported the sodium salts effectiveness of monovanadate, molybdate, and

tungstate and some derivatives of Neville-Winter acid dyes on the carbon steel corrosion in 3.5% NaCl aqueous solution. Many researches have released a wealth of information on the surfaces of metals and alloys based on the adsorption process and adsorption isotherm [14-18]. According to a review by Bathily et al., essential oils have the ability to reduce corrosion [19].

Using a methanol extract of Gongronema latifolium, the inhibitory and adsorption potentials of mild steel corrosion were reported [20]. Although, an inorganic and organic corrosion inhibitor have been used since decades and their applications right now have a serious impact. Later on, some governments restricted some of the organic and inorganic inhibitors due to their toxicity to the environment [21-24]. An imidazolinium carboxylate salt has been investigated for its potential to prevent mild steel corrosion synergistically in aqueous chloride solutions [25]. In order to increase resistance's corrosion of reinforcing steel caused in the presence of chloride in concrete pore solutions, ginger extract as an ecologically friendly inhibitor has been used [26]. Electrochemical impedance spectroscopy was employed to investigate an isothermal adsorption study on inhibitory of corrosion performance of β-cyclodextrin supported by polyacrylamide as synergistic inhibitor for X80 steel used in the industries of gas and oil [27]. It has been observed that 2-mercaptobenzimidazole and oleic imidazoline work synergistically to inhibit carbon steel corrosion in CO_2-saturated brine solutions. A combination of MBI and OIM was shown to provide an excellent synergy to mitigate corrosion of carbon steed in saturated brine solutions - carbon dioxide system [28]. Experimental and theoretical aspects into the synergistic effect of iodide ions and 1-acetyl-3-thiosemicarbazide on the corrosion protection of C1018 steel in 1 M HCl was studied [29]. Inhibition efficiency of mild steel using methylbenzyl quaternary imidazoline derivative and iodide ions as a synergistic corrosion inhibitor in H_2SO_4 solutions medium [30]. Inhibition efficiency of carbon steel corrosion in the presence of ionic liquids – iodide ions system synergistically was studied in formation water associated with crude oil and the inhibitory efficacy remarkably was observed [31]. A study focused on the combined effect of iodide ions and leaf, and stem extracts of sida acuta on suppression of MS metal corrosion in 1M H_2SO_4. Synergism was shown to be the reason behind the increased inhibitory efficacy of the leaves extracts brought about by adding the iodide ions at varying doses [32]. A mechanism of synergism of inhibitor blend based on electron transfer behavior was investigated by Han et al. [33]. Examining ginger extract as a green corrosion inhibitor of mild steel in a hydrochloric acid solution, the findings showed that the inhibition efficacy might reach up to 91% [34]. Using sodium sulphite as a standalone inhibitor, Gouda and Sayed [35] observed that, when steel was subjected to corrosion inhibition in a closed system using sodium sulphite as a corrosion inhibitor at room temperature, both total cathodic protection and the removal of O_2 from the solution were achieved.

2. METHODOLOGY AND EXPERIMENTAL WORK

2.1 Materials preparation

The coupons used in this study were typically that used in the industries of oil and gas. coupons of A333 and API 5L with the following composition (wt% maximum): 0.30-C; 0.37-Si; 0.025-P; 0.01-Al; 1.35-Mn; 0.025-S; 0.50-Ni; 0.40-Cr; 0.15-Mo; and the reminder iron were used for the corrosion tests. These coupons which were inserted into the acidic crude oil pipeline is with dimensions of 15.4 mm outside diameter, 1 mm thickness, and 5 mm length. The total acidity number for the crude oil was tested using KOH. This test indicates to the crude oil refinery the potential of corrosion problems in petroleum refinery due to existing the naphthenic acid. The acidic crude oil's pH was 5.8, crude oil with its chemical make-up in ppm was 1.9×10^4 Cl^-; 950 Ca^{2+}; 650 SO^{2-}; 450 Mg^{2+}; 64 HCO^-; 58 Na^+; and 7.06 PO^-. Sodium sulfite used as received (Sigma-Aldrich® Brand, Merck). The ginger was purchased from the local market, cleaned, cut to desired pieces, dried and crushed into a very fine powder. The prepared powder was then mixed with double distilled water in the ratio of 1g: 8 g, respectively, and then kept for 24 hours at ambient temperature. Later, the extracted solution was filtered using filtration paper and heated in the oven with a temperature of 40℃ for about 24 hours to produce ginger extract (GE) [34].

For reliable measurements of gravimetric and electrochemical of polarization and impedance, the surface of the chosen coupons was polished under running water using emery paper with grade numbers 220, 320, 450, and 600 CSI before each experiment. It was then rinsed with distilled water, dried on clean tissue paper, submerged in benzene for five seconds, dried again, and submerged in acetone for five seconds before being dried again with clean tissue paper. They were then placed in a desiccator and left running for an hour before use.

2.2 Gravimetric measure

Prior to being immersed in the acidic crude oil, the coupons initially were weighed using a balance (accuracy 0.1 mg, ABP 300-4M, weight capacity 320 g). The A333 and API 5L corrosion rates were calculated at different temperatures (40 to 80℃), specimen exposure times (24 to 172 h), inhibitor concentrations (20 - 200 ppm GE and 40 - 180 ppm SS), and velocities range of (0.8 - 2.5 m/s), using the following equation.

$$C_r = \frac{8{,}760\ M}{A \times t \times \rho} \tag{1}$$

where, C_r is the corrosion rate (mmpy), M is the lost mass [mg], t is the time interval exposure [h], A is surface area of the coupon [mm^2], and ρ is the density of the coupon [g/cm^3]. A controlled thermostat water bath (Weiber Comp. Ltd. India) was used to keep the specimens at the proper temperature. A magnetic flow meter (DN100- China) was used to regulate the required fluid velocities within the pipe. Eq. (2) may be used to calculate the inhibitor's effectiveness (η) in the gravimetric approach.

$$\eta = \frac{(C_r)_a - (C_r)_p}{(C_r)_a} \tag{2}$$

Subscript a and p represent absence and presence of the inhibitor of A333/API 5L.

2.3 Electrochemical and polarization measurements

2.3.1 Linear polarization resistance test

A standard cylindrical glass cell with three electrodes was used to conduct electrochemical trends in a dynamic flow process piping. A cylinder made of A333/API 5L with 15.4

mm outside diameter, 1 mm in thickness, and 5 mm in length, as the working electrode. A solution of 0.02 M acidic crude oil with different velocities was the medium for the exterior and interior surface area of the working electrode, which was fixed inside the pipe by inserting a probe into the pipe of acidic crude flow. Platinum and saturated calomel electrodes (SCEs) are the counter and reference electrodes, respectively. The polarization Tafel slope curves were recorded at 0.2 mV/s scan rate using a potentiostat/galvanostat type of GAMRY v6.33. Following a 30-minute exposure to corrosion potential, the A333 and API 5L electrode was subjected to a 10-minute pre-polarization at a potential of -800 mV. At this level, the working electrode exhibited uniform polarization. To anodic potentials, the potential was swept. Throughout the experiment, both with and without inhibitors, acidic crude oil was used to aerate the test fluid in the cell. With ± 10 mV amplitude signal, the AC impedance spectroscopy measurements were implemented at corrosion potential throughout 10 kHz to 0.05 Hz frequency. I_{cor} may be calculated as follows using the Stern-Geary equation. Using Tafel slopes of the anodic and cathodic, the corrosion current density (I_{cor}) could be calculated as follows:

$$I_{cor} = \frac{b_a\, b_c}{2.303\,(b_a + b_c) \times R_{ct}} \tag{3}$$

where, b_c and b_a are Tafel slopes (mV/decade) of the cathodic and anodic reactions, respectively and R_{ct} (Ω) is the transfer resistance charge. The inhibitory efficacy could be then determined as the equation below:

$$\eta = \frac{(I_{cor})_a - (I_{cor})_p}{(I_{cor})_a} \tag{4}$$

where, $(I_{cor})_a$ and $(I_{cor})_p$ are the corrosion current density (μA/m^2) in absence and presence of inhibitors prepared, respectively.

The corrosion rate (C_r) can be determined in term of corrosion current density as the following:

$$C_r = \frac{8.954 \times 10^{-3} \times I_{cor} \times M}{z\,\rho} \tag{5}$$

where, M is the molar mass of the specimen (g/mol), z is the electron transfer valence, and ρ is the specimen density (g/cm^3).

2.3.2 Electrochemical impedance spectroscopy (EIS)

The EIS studies were carried out in a dynamic three-necked cell. The coupons cut from a new pipe, saturated calomel, and platinum foil, are working electrode, reference electrode, and counter electrodes, respectively, in acidic crude oil with and without inhibitor.

A potentiostat/galvanostat (GAMRY IMX8, 8 channels for measurement, compliance current ± 30 mA @ 500 Ω load) with low noise signal, high speed current, high sensitivity, and simple front panel operation was employed. A frequency analyzer system type Solartron model 1250 was linked with CorrWare software and GPIB and RS232 interfaces. Using a frequency between 10 kHz and 0.05 kHz, as well ± 10 mV as signal amplitude, AC measurements of impedance spectroscopy were scanned for the corrosion potential. The charge transfer resistance (R_{ct}), the solution resistance (R_s), and the double layer capacitance (C_{dl}) as equivalent circuit are depicted in Figure 2.

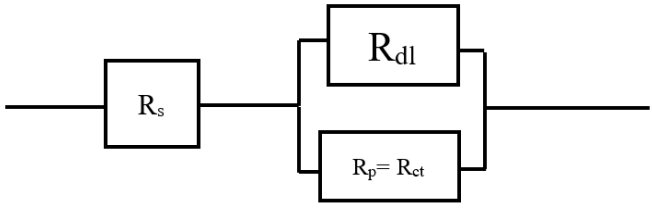

Figure 2. Equivalent circuit chart

The impedimetric data validity can be further evaluated by using the Kramers-Kronig relations to calculate the real and imaginary part as the following equations:

$$Z'(\omega) = R_s + \frac{2}{\pi}\int_0^{\infty} \frac{x\,Z''(x) - \omega\,Z''(\omega)}{x^2 - \omega^2}\,dx \tag{6}$$

$$Z''(\omega) = \frac{2\omega}{\pi}\int_0^{\infty} \frac{Z'(x) - Z'(\omega)}{x^2 - \omega^2}\,dx \tag{7}$$

Finally, the impedance in the form of real and imaginary parts is:

$$Z(\omega) = Z'(\omega) - j\,Z''(\omega) \tag{8}$$

$$Z(\omega) = R_s + \frac{R_{ct}}{1 + (\omega\,R_{ct}C_{dl})^2} - j\,\frac{\omega\,{R_{ct}}^2 C_{dl}}{1 + (\omega\,R_{ct}C_{dl})^2} \tag{9}$$

where,

$$C_{dl} = \frac{1}{2\,\pi\,f_{max}\,R_{ct}} \tag{10}$$

Nyquist plots that represent the impedance diagrams are considered. The surface coverage degree using charge transfer resistance in the absence and presence the inhibitor could be obtained as following equation:

$$\eta = \frac{\left(\frac{1}{R_{ct}}\right)_a - \left(\frac{1}{R_{ct}}\right)_p}{\left(\frac{1}{R_{ct}}\right)_a} \tag{11}$$

2.4 Fluid velocity influence

An electromagnetic flow meter was used to specify the fluid velocity inside the cell of test which was adopted by connecting it with circulating 20 mm inside diameter via electromagnetic sensor of magnetic flow meter. As the fluid flows through the magnetic field, and due to existing two potential electrodes inside the pipe perpendicular to the flow, the voltage would be induced is directly proportional to the fluid velocity (v) in m/s. Faraday's principle can be obtained:

$$v = \frac{E}{k\,B\,d} \tag{12}$$

where, E is the voltage induced (Volt), k is the sensitivity meter constant, B is the magnetic field density (Wb/m^2), and d is the diameter of the conductor (m) (here it is the pipe diameter). A silent type magnetic pressure pumps not exceeding 67 dB were used.

3. RESULTS AND DISCUSSIONS

3.1 Gravimetric measurements

The corrosion rate and inhibition efficiency values obtained from A333 and API 5L mass loss experiments at temperature ranges of 40 to 80℃, different inhibitor concentration of individual SS and then combination of GE and SS at different fluid velocities (0.85, 1.5, and 2.5 m/s) in acidic crude oil medium as displayed in Table 1. Beyond this concentration, the operation will be cost- effective consideration. The error and deviation of the replicate's experiments is depicted in Figure 3 elaborating that the deviation is in acceptable range.

Table 1. A333/API L5 corrosion rate and surface coverage in 0.02 M crude oil at different concentrations of SE-SS and temperatures, at 1.5 m/s optimum fluid velocity

Temperature (℃)	Concentration (ppm)		*CR* (mmpy)	*η* %
	Sodium Sulfite	Ginger Extract		
40	blank	blank	0.9462	----
	40	–	0.7387	21.93
	50	–	0.5871	37.95
	70	–	0.3508	62.93
	120	–	0.3244	65.72
	180	–	0.2362	75.04
50	blank	blank	0.9862	----
	40	20	0.5716	42.04
	50	40	0.4172	57.70
	70	70	0.3541	64.09
	120	130	0.2026	79.45
	180	200	0.1671	83.05
60	blank	blank	1.0567	----
	40	20	0.6358	39.83
	50	40	0.4168	57.74
	70	70	0.3557	63.93
	120	130	0.2171	77.98
	180	200	0.1764	82.11
70	blank	blank	1.1014	----
	40	20	0.6640	39.71
	50	40	0.4368	60.34
	70	70	0.3592	67.39
	120	130	0.2166	80.34
	180	200	0.1800	83.66
80	blank	blank	1.1541	----
	40	20	0.6680	42.12
	50	40	0.4359	55.80
	70	70	0.3691	62.57
	120	130	0.2237	77.32
	180	200	0.1892	80.81

The efficiency of SS inhibitor alone is significantly lower than that of the synergistic inhibitor supported by GE. The lower efficiency in the individual SS might be resulted due to the existing of cathodic and anodic cells which occurred due to the weak and porous film formed on the metal surface where localized corrosion takes place. Absolutely, at increasing of synergistic inhibitor concentration, the corrosion inhibition increased. The optimum concentration of SS-GE to obtain the highest efficiencies were 180 and 200 ppm, respectively. The increase in η in the presence GE-SS could be attributed that the synergistic mechanism of the presence of =O, -OH, and -O- groups, flavonoids, and amino acids in GE enhancing adsorption phenomenon on the metal surface, as well, SS donates the electrons from $-SO_3$ group to the metal surface making the surface more negative where the GE species could be readily adsorbed. Moreover, this process is facilitated by the presence of vacant orbital of low energy in iron atom (main metal of coupon used in this study) as observed in the transition elements.

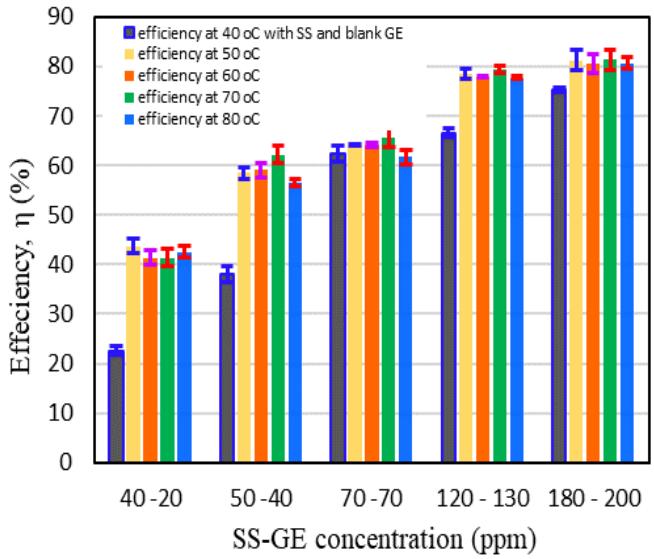

Figure 3. Weight loss of A333/API L5 in acidic crude oil solution in the presence of different concentration of SS-GE inhibitor different temperature and 1.5 m/s

3.2 Potentiodynamic polarization (linear polarization resistance)

The Tafel cathodic and anodic polarization curves of an A333 / API 5L electrode in acidic crude oil, without and with different concentrations of SS and GE acting as a synergistic inhibitor, are shown in Figure 4.

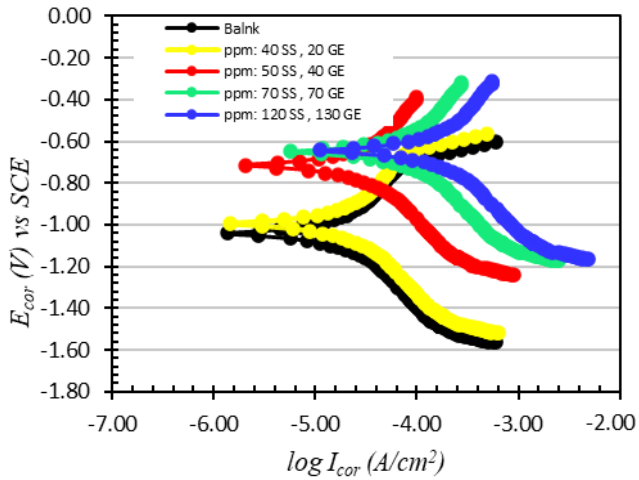

Figure 4. Potentiodynamic polarization curves for A333/API L5 in acidic crude oil solution in presence and absence of different concentration of SS-GE inhibitor at 40℃ and 1.5 m/s

The suggested inhibitor could play a significant role to changes the cathodic and anodic slopes to the lower corrosion current for both the cathodic and anodic curves. Increasing the inhibitors concentrations led to decrease both the anodic and cathodic corrosion current curves; however, the anode curves show the greater impact. The aforementioned behavior indicates that the presence of this type of the inhibitors slows the hydrogen evolution process at the cathodic as well as

anodic dissolution got down impact.

Table 2 displays the corrosion potential (E_{cor}), corrosion current density (I_{cor}), and inhibitor performance (η) values for the corrosion of A333 and API 5L in acidic crude oil at different temperatures and inhibitor concentrations. It is shown that, the addition of the inhibitor causes minor modifications in the corrosion potential towards the positive charge. In addition, around 1.5 m/s, there is a little shift in E_{cor}. As a result, it may be concluded that the inhibitor's absorbed molecules have no impact on the process behind hydrogen evolution [13].

SS by virtue of its capacity maintains the values of pH in the between 6.5 to 7.6 [5]. The use of small quantities of SS with GE in recirculating acidic crude oil system may eliminate the rusting by forming a passive film by SS and adsorbed species by GE on the metal surface. It is obvious that the interaction of Tafel lines slope shifted to less current with the increase of SS-GE blend. This indicates that, the protection efficiency increased with increasing concentration of the synergistic GE and SS is the critical value. It is also shown that, the cathodic branches control the reaction, i.e., SS-GE acts as cathodic inhibitors.

Table 2. E_{cor}, I_{cor}, R_{ct}, C_{dl} and η of A333 and API 5L in 0.02 M crude oil at different concentrations of SS-GE and temperatures at 1.5 m/s optimum fluid velocity

Temperature (°C)	Concentration (ppm)		LPR			EIS		
	Na_2SO_3	Ginger Extract	E_{cor} (mV)	I_{cor} (A/cm^2)	η	R_{ct} (Ω/cm^2)	η %	C_{dl} (μF/cm^2)
40	Blank	blank	-497	8.45E-05	–	110.46		137.29
	40	–	-489	5.85E-05	30.77	156.35	29.35	113.79
	50	–	-480	3.60E-05	57.42	189.58	41.73	93.85
	70	–	-486	3.03E-05	64.15	242.46	54.44	73.38
	120	–	-500	2.86E-05	66.19	287.59	61.59	61.86
	180	–	-499	1.90E-05	77.49	378.74	70.83	46.98
50	blank	blank	-537	9.560E-05		107.31		141.32
	40	20	-458	5.380E-05	43.72	201.05	46.63	88.49
	50	40	-460	3.475E-05	63.65	270.67	60.35	65.73
	70	70	-453	2.869E-05	69.99	332.52	67.73	53.51
	120	130	-455	9.980E-06	88.56	698.66	84.64	25.47
	180	200	-450	9.043E-06	89.54	798.72	86.56	22.28
60	blank	blank	-543	1.004E-04		106.63		142.22
	40	20	-502	6.000E-05	40.24	200.47	46.81	88.75
	50	40	-502	3.450E-05	63.91	271.6	60.74	65.51
	70	70	-487	2.569E-05	73.13	372.69	71.39	47.74
	120	130	-488	1.230E-05	87.13	698.42	84.72	25.49
	180	200	-489	1.012E-05	89.41	797.66	86.63	22.30
70	blank	blank	-579	1.234E-04		106.87		141.90
	40	20	-510	7.340E-05	40.52	199.04	46.31	89.39
	50	40	-510	4.280E-05	65.32	266.89	59.58	66.66
	70	70	-519	3.433E-05	72.18	370.61	70.89	48.01
	120	130	-496	1.900E-05	84.60	694.37	84.47	25.62
	180	200	-495	1.390E-05	88.74	786.84	86.29	22.61

3.3 Electrochemical impedance spectroscopy (EIS)

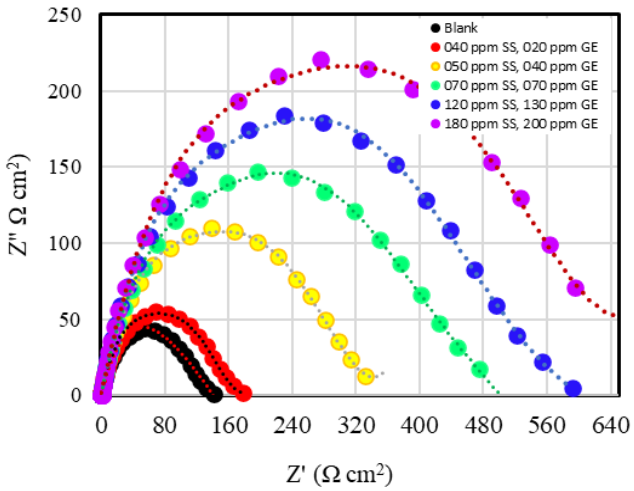

Figure 5. Nyquist semicircle of A333 in acidic crude oil at different dosages of SS and GE, at 40°C and velocity of 1.5 m/s

Nyquist plots (Figure 5), where notably shows the same pattern performance, explaining that the semicircle diameter grows by increasing the concentration of GE and SS. This is ascribed to the inorganic inhibitor's passive layer development of SS on the metal surface as well as the existence of aromatic group on the GE. Additionally, the combination inhibitor of SS and GE functions as an oxygen scavenger to prevent corrosion by blocking the oxygen-cathodic area, raising surface impedance, and makes the R_s is high, and limiting the diffusion of reducible species to these regions. Table 2 displays the inhibitor concentrations and parameters of impedance and polarization.

When comparing the combination of SS and GE under the same conditions to SS alone, the former displayed lower values of corrosion current density (I_{cor}) and C_r, and higher values of R_{ct}.

This occurs because, particularly at high flow velocities, the layer that forms on the metal surface is not very adhesive. As it may be the inhibitor is not present in sufficient quantity at the corrodible surface, especially at high fluid velocities, which causes pitting corrosion on the metal surface.

3.4 Effect of temperature

Table 2 illustrates how temperature affects the rate of corrosion of A333 and API 5L in acidic crude oil in the absence and presence of various concentrations of SS and GE in terms of Tafel slope, corrosion current, and corrosion

potential. The effect temperature can be estimated by determination of the activation energy, enthalpy, and entropy for adsorption process on A333 and API 5L using the Arrhenius and Eyring equations in Eqs. (13) and (14) as the following:

$$I_{cor} = k \exp\left(\frac{-\Delta E_a}{R\,T}\right) \quad (13)$$

$$\Delta H_a = \Delta\, E_a - R\,T \quad (14)$$

ΔE_a is the change in activation energy, k is constant, R is 8.314 J/mol K and T is the absolute temperature. Using Arrhenius plot of the corrosion rate of A333/API 5L at optimum velocity of 1.5 m/s is plotted in Figure 6. Plots of *ln* (I_{cor}) *1/T*, obtains the activation energy values, E_a and pre-exponential factor, k at different inhibitor concentration and the parameters of activation, enthalpy, and entropy energies are depicted in Table 3. For A333 and API 5L, thus, k predominantly determines the reduction in corrosion current. An increase in inhibitor concentration, the values of k declined noticeably. Also, a strong chemisorption connection between the inhibitor and the metal is most likely present since the lowering and fluctuation values of E_a at higher concentration in the medium relative to an unfettered one might the reason.

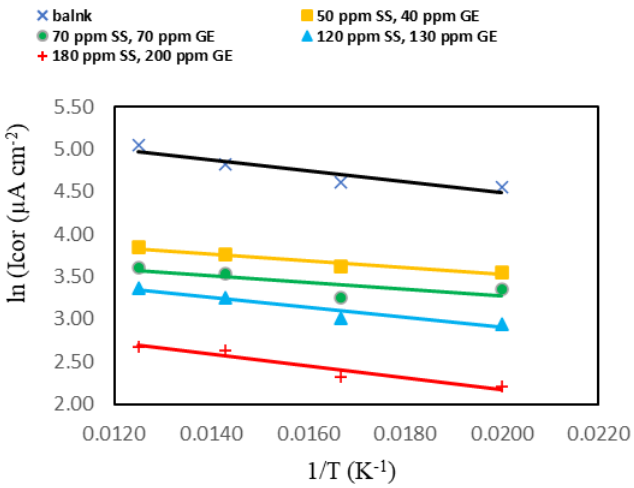

Figure 6. Arrhenius plots of corrosion current of A333 /API 5L in acidic crude oil in the absence and presence of various concentrations of SS and GE at different temperature and at 1.5 m/s

Table 3. Energy parameters for A333 and API 5L in 0.02 M crude oil at different dosages of SS-GE at different temperatures at 1.5 m/s optimum velocity

Concentration SS-GE (ppm)	k (µA/cm²)	ΔE_a (kJ/mol)	ΔH_a (kJ/mol)	ΔS_a J/mol·K
40 – 20	323.02	166.99	164.39	-342.36
50 – 40	75.94	107.65	104.97	-342.80
70 – 70	56.86	105.59	102.82	-343.13
120 – 130	59.00	167.68	164.83	-344.57
180 – 200	58.59	159.82	148.57	-344.85

An alternative Arrhenius formula can give more details:

$$I_{cor} = \frac{R\,T}{N\,h}\exp\left(\frac{\Delta S}{R}\right)\exp\left(\frac{-\Delta H}{R\,T}\right) \quad (15)$$

where, h is Planck's constant, N is Avogadro's number, ΔS_a is the entropy of activation, and ΔH_a is the enthalpy of activation. Plotting of *ln* (I_{cor}/T) as y-axis and 1/T as x-axis as shown in Figure 7, obtaining a straight line with a slope of [$\Delta H_a/(R)$] and intercepts of [*ln* (R/Nh) + $\Delta S_a/(R)$]. Further, the values of ΔH_a obtained from the slopes of Eq. (14) the values obtained are in good agreement with each other.

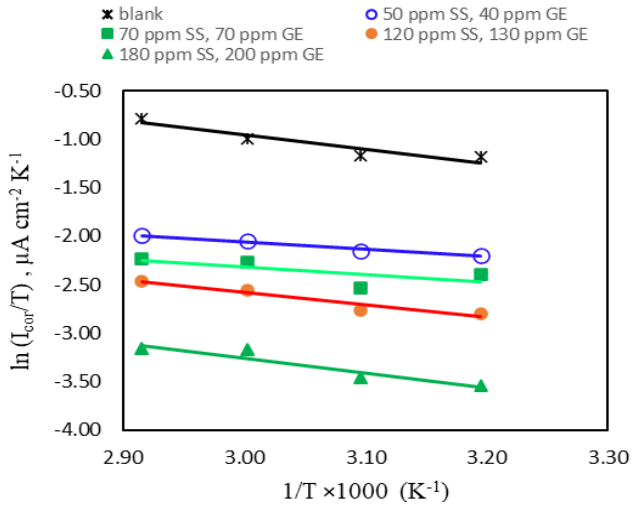

Figure 7. Arrhenius alternative plots of corrosion current of A333 and API 5L in acidic crude oil in the absence and presence of various concentrations of SS and GE at different temperature and at 1.5 m/s

Data collected show that the thermodynamic parameters of A333 and API 5L reaction in the acidic crude oil in the existence of GE inhibitor synergistically with SS are lower than that of the solution inhibitor free. The reaction between the medium and the metal is endothermic due to +ve of ΔH_a, elaborating that the dissolution of A333 and API 5L is complicated. Whereas, -ve of entropy and negatively increasing in the presence of inhibitor resulting that the film adsorbed on the metal is stable because of the functional groups of GE aforementioned in this paper as well as SS donates the electron of -SO_3 group into the vacancy orbital of the metal surface A333 and API 5L.

3.5 Thermodynamic adsorption mechanism

Using thermodynamic equilibrium coefficients obtained at various temperatures and concentrations. An adsorption thermodynamics parameters were calculated to confirm the potential adsorption processes of the species adsorbed by unit area of the metal surface from solution environment, disclosing the mechanism of SS and GE as synergistic inhibitor in the medium of acidic crude oil over A333 and API 5L surface.

The experimental results were examined in conjunction with different models of adsorption isotherms, such as Langmuir, Freundlich and Temkin isotherm, to identify the appropriate fitting model that strongly describes the process adheres in order to obtain additional details.

$$\eta = K_{ads}\, C^{\frac{1}{n}} \quad (16)$$

$$ln\,\eta = ln\,K_{ads} + \frac{1}{n} ln\,C \quad (17)$$

Figure 8 reflects plotting of *ln η* versus *ln C*, which results in a straight line with the slope of 1/n and intercept *ln* K_{ads}, the linear regression coefficients (R^2) which are close to 1 confirming that, the adsorption of SS-GE on A333-API L5 surface in acidic crude oil obeys Freundlich adsorption isotherm at all temperatures studied. The equilibrium adsorption constant (K_{ads}) is related to the standard Gibbs free energy of adsorption, ΔG, absolute temperature, and universal gas constant as the following equation:

$$k_{ads} = exp\left(\frac{-\Delta G_{ads}}{R\,T}\right) \quad (18)$$

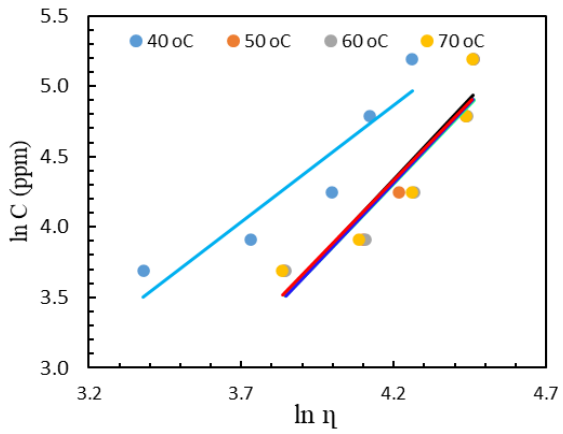

Figure 8. Freundlich adsorption isotherm of SS-GE on A333 steel surface in acidic crude oil at different temperatures and at 1.5 m/s

The parameters of adsorption thermodynamics, ΔH_{ads} and ΔS_{ads} could be obtained from Eqs. (18)-(20).

$$\Delta G_{ads} = \Delta H_{ads} - T\,\Delta S_{ads} \quad (19)$$

$$\ln k_{ads} = \frac{-\Delta H_{ads}}{R\,T} + \frac{\Delta S_{ads}}{R} \quad (20)$$

Plots of *ln* K_{ads} against 1/T for SS-GE on A333-API L5 are shown in Figure 9. The resulting lines show an intercept of ($\Delta S_{ads}/R$) and a slope of (ΔH_{ads})/R). Table 4 lists the K_{ads}, ΔG_{ads}, ΔH_{ads}, and ΔS_{ads} values. The negative values of ΔG_{ads} indicates that adsorption process is spontaneity and the persistence of the layer to be adsorbed on the A333/API L5 surface.

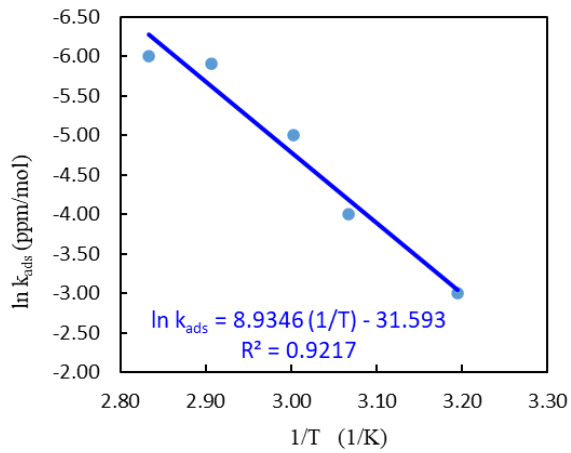

Figure 9. *ln* K_{ads} vs 1/T for A333-API L5 in the presence SS-GE

Table 4. Thermodynamic characteristics of the acidic crude oil adsorption process on A333 surface, as determined by polarization at various temperatures and at 1.5 m/s

T (K)	K_{pas} (L/mg)	*1/n*	R^2	ΔG_{ads} (kJ/mol)	ΔH_{ads} (kJ/mol)	ΔS_{ads} J/(mol·K)
313	0.122432	1.700	0.87	5.465		
323	0.005021	2.294	0.9	14.217		
333	0.006461	2.320	0.88	13.959	-74.28	-262.66
343	0.005574	2.262	0.87	14.799		
353	0.005763	2.253	0.89	15.133		

It seems that ΔG_{ads} does not exceed 20 kJ which is consistent with physisorption, or electrostatic bonds between metal surface and charged molecules, whereas 40 kJ or higher indicates the chemisorption, or sharing the charge or transfer of inhibitor molecules to the metal surface to form a coordinate type of bond [5]. Accordingly, the values of ΔG_{ads} that were obtained indicate that physisorption is the mode of adsorption for SS-GE on A333-API L5 steel, as well the higher negative value of entropy means the sorption is strong and not arbitrary. In spite our data processing of adsorption isotherm obeys Freundlich isotherm, obviously experimental data of this results (Figure 8), it is found that the more fitting in the presence of synergistic inhibitors is less than that of the individual inhibitor. Very rare searchers [34, 35] for individual SS and GE as corrosion inhibitors have studied them individually the inhibition efficiency on the mild steel, it is noticeable that the adsorption isotherm parameters are less than the adsorption isotherm parameter in the current study as synergy. Moreover, Table 2 shows the surface coverage of individual and synergistic are 70.83 % and 86.56 %, respectively, giving the synergistic parameter is more than unity stating that the combination is successful. This may be attributed to the presence of the -SO_3 group in SS that donates its elections to the metal surface changing it to cathodic, as well enhances GE to be adsorbed on the metal surface due to the vacancy orbital of the metals.

The adsorption of any inhibitor on the metal surface especially organic compounds containing groups of = O, -OH which exists in GE retards the corrosion action of metal.

3.6 Effect of fluid velocity

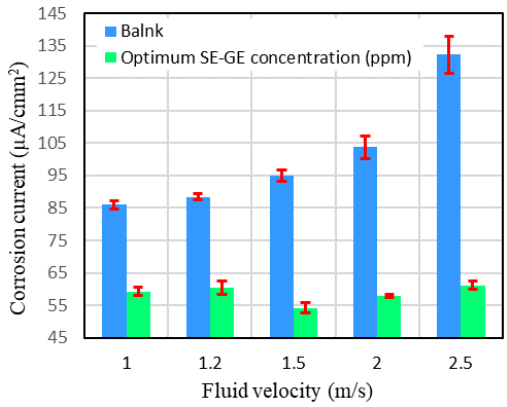

Figure 10. Corrosion current vs fluid velocity at blank and optimum amount of SS-GE on A333-API L5 steel at 40°C

I_{cor} is plotted as a function of velocity in both blank and the optimum concentration of SS-GE at 50°C as shown in Figure 10. The error and deviation are resulted from three replicating experiments, and the error bar reveal an acceptable range. The

error values in the absence of the inhibitors remarkably are high, in contrast in the presence of optimum amount of the inhibitors. In the absence of an inhibitor, I_{cor} elevated significantly as fluid velocity increased, but it appears to have marginally risen in the presence of an inhibitor. At 1.5 m/s, the greatest inhibitory effectiveness was noted. This is because an appropriate enhance of minimum velocity is required to ensure that the inhibitor is distributed evenly and also that the suspended particles do not precipitate on the metal surface, mitigates the potential erosion or pitting corrosion on the metal.

4. CONCLUSIONS

In this study, in the acidic crude oil media, A333 and API 5L has been inhibited by GE inhibitor that and SS that work synergistically to mitigate the medium corrosivity. Temperature, inhibitor concentration, and fluid velocity have significant effect on the inhibition efficiency and adsorption isotherm; however, the concentration is dominant. In the ideal circumstances, the suggested inhibitor for A333 and API 5L has the inhibition efficiency as average of 86.56 % in terms of corrosion current. The synergism parameter which could be determined from tabulated data for the current study for different concentrations of SS and GE has been found to be greater than unity revealing that the synergistic of the combination of GE and SS successfully takes place. The error deviation in the blank concentration was notably high in contrast with those in the presence of inhibitor blend of SS-GE.

The values of thermodynamics adsorption isotherm indicates that, the adsorption processes of inhibitor on A333 and API 5L acidic crude oil media are mixed between physisorption and chemisorption. There is a good agreement correlation between the mass loss and the electrochemical polarization data. The oscillating of the activation energy with increasing the concentration of inhibitors elaborates the changes in energy required for the film formed on the metal surface, this phenomenon is enhanced by the increase of entropy negatively in the presence of inhibitor which indicates the stability of the film formed.

The limitation of this corrosion inhibitors (GE-SS) that at high temperature (Table 2) and high velocity (included only at 1.5 m/s) its performance decreased slightly. As SS is inorganic inhibitor, so it should be concentration enough to change the anodic current density to cathodic current density. A small amount of an inorganic inhibitors affects the film formed on the metal surface to being not uniform leading to a localized corrosion occurs. We found an increase of further concentrations of both inhibitors are negatively cost-effective consideration.

REFERENCES

[1] Mohana, K.N., Badiea, A.M. (2008). Effect of sodium nitrite–borax blend on the corrosion rate of low carbon steel in industrial water medium. Corrosion Science, 50(10): 2939-2947. https://doi.org/10.1016/j.corsci.2008.07.002

[2] Loto, R.T., Solomon, M.M. (2023). Application of ginger and grapefruit essential oil extracts on the corrosion inhibition of mild steel in dilute 0.5 M H2SO4 electrolyte. Scientific African, 19: e01489. http://creativecommons.org/licenses/by-nc-nd/4.0/.

[3] Badiea, A.M., Mohana, K.N. (2009). Effect of temperature and fluid velocity on corrosion mechanism of low carbon steel in presence of 2-hydrazino-4, 7-dimethylbenzothiazole in industrial water medium. Corrosion Science, 51(9): 2231-2241. https://doi.org/10.1016/j.corsci.2009.06.011

[4] Medupin, R.O., Ukoba, K.O., Yoro, K.O., Jen, T.C. (2023). Sustainable approach for corrosion control in mild steel using plant-based inhibitors: A review. Materials Today Sustainability, 22: 100373. https://doi.org/10.1016/j.mtsust.2023.100373

[5] Dehghani, A., Mostafatabar, A.H., Ramezanzadeh, B. (2023). Synergistic anticorrosion effect of Brassica Hirta phytoconstituents and cerium ions on mild steel in saline media: Surface and electrochemical evaluations. Colloids and Surfaces A: Physicochemical and Engineering Aspects, 656: 130503. https://doi.org/10.1016/j.colsurfa.2022.130503

[6] Royani, A., Hanafi, M., Manaf, A. (2022). Prospect of plant extracts as eco-friendly biocides for microbiologically influenced corrosion: A review. International Journal of Corrosion and Scale Inhibition, 11(3): 862-888. https://doi.org/10.17675/2305-6894-2022-11-3-1

[7] Ramezanzadeh, M., Bahlakeh, G., Ramezanzadeh, B. (2019). Study of the synergistic effect of Mangifera indica leaves extract and zinc ions on the mild steel corrosion inhibition in simulated seawater: Computational and electrochemical studies. Journal of Molecular Liquids, 292: 111387. https://doi.org/10.1016/j.molliq.2019.111387

[8] Othman, N.K., Yahya, S., Ismail, M.C. (2019). Corrosion inhibition of steel in 3.5% NaCl by rice straw extract. Journal of Industrial and Engineering Chemistry, 70: 299-310. https://doi.org/10.1016/j.jiec.2018.10.030

[9] Royani, A., Aigbodion, V.S., Hanafi, M., Mubarak, N.M., Verma, C., Alfantazi, A., Manaf, A. (2023). Enhancing the corrosion inhibition performance of Tinospora cordifolia extract using different fractions of methanol solvent on carbon steel corrosion in a seawater-simulated solution. Applied Surface Science Advances, 18: 100465. https://doi.org/10.1016/j.apsadv.2023.100465

[10] Badiea, A.M., Mohana, K.N. (2008). Effect of fluid velocity and temperature on the corrosion mechanism of low carbon steel in industrial water in the absence and presence of 2-hydrazino benzothiazole. Korean Journal of Chemical Engineering, 25: 1292-1299. http://doi.org/10.1007/s11814-008-0212-1

[11] Badiea, A.M., Mohana, K.N. (2009). Corrosion mechanism of low-carbon steel in industrial water and adsorption thermodynamics in the presence of some plant extracts. Journal of Materials Engineering and Performance, 18: 1264-1271. http://doi.org/10.1007/s11665-009-9378-x

[12] Al-Amiery, A.A., Isahak, W.N.R.W., Al-Azzawi, W.K. (2023). Corrosion inhibitors: Natural and synthetic organic inhibitors. Lubricants, 11(4): 174. https://doi.org/10.3390/lubricants11040174

[13] Abdallah, M., El-Etre, A.Y., Soliman, M.G., Mabrouk, E.M. (2006). Some organic and inorganic compounds as inhibitors for carbon steel corrosion in 3.5 percent NaCl solution. Anti-corrosion Methods and Materials, 53(2): 118-123. http://doi.org/10.1108/00035590610650820

[14] Dlouhy, M., Kokalj, A. (2022). How adsorbed H, O, OH, and Cl affect plain adsorption of imidazole on copper. Corrosion Science, 205: 110443. https://doi.org/10.1016/j.corsci.2022.110443
[15] Kokalj, A. (2023). On the use of the Langmuir and other adsorption isotherms in corrosion inhibition. Corrosion Science, 217: 111112. https://doi.org/10.1016/j.corsci.2023.111112
[16] Turano, M., Walker, M., Grillo, F., Gattinoni, C., Hunt, G., Kirkman, P., Richardson, V., Baddeley, C.J., Costantini, G. (2022). Adsorption of the prototypical organic corrosion inhibitor benzotriazole on the Cu (100) surface. Corrosion Science, 207: 110589. https://doi.org/10.1016/j.corsci.2022.110589
[17] Kokalj, A. (2023). On the estimation of standard adsorption free energy from corrosion inhibition efficiencies. Corrosion Science, 217: 111139. https://doi.org/10.1016/j.corsci.2023.111139
[18] Kokalj, A. (2023). A general-purpose adsorption isotherm for improved estimation of standard adsorption free energy. Corrosion Science, 217: 111124. https://doi.org/10.1016/j.corsci.2023.111124
[19] Bathily, M., Ngom, B., Gassama, D., Tamba, S. (2021). Review on essential oils and their corrosion-inhibiting properties. American Journal of Applied Chemistry, 9(3): 65-73. https://doi.org/10.11648/j.ajac.20210903.12
[20] Aralu, C.C., Chukwuemeka-Okorie, H.O., Akpomie, K.G. (2021). Inhibition and adsorption potentials of mild steel corrosion using methanol extract of Gongronema latifoliuim. Applied Water Science, 11(2): 1-7. http://doi.org/10.1007/s13201-020-01351-8
[21] Dariva, C.G., Galio, A.F. (2014). Corrosion inhibitors–principles, mechanisms and applications. In Developments in Corrosion Protection, BoD – Books on Demand, pp. 365-378. http://doi.org/10.5772/57255
[22] Kuznetsov, Y. I. (2013). Organic inhibitors of corrosion of metals. Springer Science & Business Media. http://doi.org/10.1007/978-1-4899-1956-4
[23] Loto, R.T., Loto, C.A. (2012). Effect of P-phenylediamine on the corrosion of austenitic stainless steel type 304 in hydrochloric acid. International Journal of Electrochemical Science, 7(10): 9423-9440. https://doi.org/10.1016/S1452-3981(23)16208-0
[24] Loto, R.T. (2017). Corrosion inhibition studies of the combined admixture of 1, 3-diphenyl-2-thiourea and 4-hydroxy-3-methoxybenzaldehyde on mild steel in dilute acid media. Revista Colombiana de Química, 46(1): 20-32. https://doi.org/10.15446/rev.colomb.quim.v46n1.59578
[25] Chong, A.L., Mardel, J.I., MacFarlane, D.R., Forsyth, M., Somers, A.E. (2016). Synergistic corrosion inhibition of mild steel in aqueous chloride solutions by an imidazolinium carboxylate salt. ACS Sustainable Chemistry & Engineering, 4(3): 1746-1755. https://doi.org/10.1021/acssuschemeng.5b01725
[26] Liu, Y.Q., Song, Z.J., Wang, W.Y., Jiang, L.H., Zhang, Y.J., Guo, M.Z., Song, F.Y., Xu, N. (2019). Effect of ginger extract as green inhibitor on chloride-induced corrosion of carbon steel in simulated concrete pore solutions. Journal of Cleaner Production, 214: 298-307. https://doi.org/10.1016/j.jclepro.2018.12.299
[27] Wang, C., Zou, C., Cao, Y. (2021). Electrochemical and isothermal adsorption studies on corrosion inhibition performance of β-cyclodextrin grafted polyacrylamide for X80 steel in oil and gas production. Journal of Molecular Structure, 1228: 129737. https://doi.org/10.1016/j.molstruc.2020.129737
[28] Wang, X., Yang, J., Chen, X., Ding, W. (2022). Synergism of 2-mercaptobenzimidazole and oleic imidazoline on corrosion inhibition of carbon steel in CO_2-saturated brine solutions. Journal of Molecular Liquids, 368: 120645. https://doi.org/10.1016/j.molliq.2022.120645
[29] Alamri, A.H. (2020). Experimental and theoretical insights into the synergistic effect of iodide ions and 1-acetyl-3-thiosemicarbazide on the corrosion protection of C1018 carbon steel in 1 M HCl. Materials, 13(21): 5013. https://doi.org/10.3390/ma13215013
[30] Okafor, P.C., Zheng, Y. (2009). Synergistic inhibition behaviour of methylbenzyl quaternary imidazoline derivative and iodide ions on mild steel in H_2SO_4 solutions. Corrosion Science, 51(4): 850-859. https://doi.org/10.1016/j.corsci.2009.01.027
[31] Abd El Wanees, S., Kamel, M.M., Ibrahim, M., Rashwan, S.M., Atef, Y., Abd Elsadek, M.G. (2024). Corrosion inhibition and synergistic effect of ionic liquids and iodide ions on the corrosion of C-steel in formation water associated with crude oil. Journal of Umm Al-Qura University for Applied Sciences, 10(1): 107-119. https://doi.org/10.1007/s43994-023-00084-z
[32] Eduok, U.M., Umoren, S.A., Udoh, A.P. (2012). Synergistic inhibition effects between leaves and stem extracts of Sida acuta and iodide ion for mild steel corrosion in 1 M H_2SO_4 solutions. Arabian Journal of Chemistry, 5(3): 325-337. https://doi.org/10.1016/j.arabjc.2010.09.006
[33] Han, P., He, Y., Chen, C.F., Yu, H.B., Liu, F., Yang, H., Zheng, Y.J. (2016). Study on synergistic mechanism of inhibitor mixture based on electron transfer behavior. Scientific Reports, 6(1): 33252. https://doi.org/10.1038/srep33252
[34] Fidrusli, A., Suryanto, Mahmood, M. (2018). Ginger extract as green corrosion inhibitor of mild steel in hydrochloric acid solution. In IOP conference Series: Materials Science and Engineering, Kuala Lumpur, Malaysia, Vol. 290, pp. 012087. https://doi.org/10.1088/1757-899X/290/1/012087
[35] Gouda, V.K., Sayed, S.M. (1973). Corrosion inhibition of steel by sodium sulphite. Corrosion Science, 13(9): 653-658. https://doi.org/10.1016/S0010-938X(73)80036-8